The ac stark shift and space-borne rubidium atomic clocks

Journal of Applied Physics

The ac stark shift and space-borne rubidium atomic clocks

Cite as: J. Appl. Phys. **120**, 194501 (2016); https://doi.org/10.1063/1.4967787
Submitted: 29 August 2016 . Accepted: 15 October 2016 . Published Online: 17 November 2016

V. Formichella, J. Camparo, I. Sesia, G. Signorile, L. Galleani, M. Huang, and P. Tavella

JOURNAL OF APPLIED PHYSICS **120**, 194501 (2016)

The ac stark shift and space-borne rubidium atomic clocks

V. Formichella,[1,2] J. Camparo,[3] I. Sesia,[1] G. Signorile,[1] L. Galleani,[2] M. Huang,[3] and P. Tavella[1]

[1]*INRiM – Istituto Nazionale di Ricerca Metrologica, Department of Physical Metrology, Strada delle Cacce 91, 10135 Torino, Italy*

[2]*Politecnico di Torino, Department of Electronics and Telecommunications, Corso Duca degli Abruzzi, 24, 10129 Torino, Italy*

[3]*The Aerospace Corporation, Physical Sciences Laboratories, 2310 E. El Segundo Blvd., El Segundo, California 90245, USA*

(Received 29 August 2016; accepted 15 October 2016; published online 15 November 2016)

Due to its small size, low weight, and low power consumption, the Rb atomic frequency standard (RAFS) is routinely the first choice for atomic timekeeping in space. Consequently, though the device has very good frequency stability (rivaling passive hydrogen masers), there is interest in uncovering the fundamental processes limiting its long-term performance, with the goal of improving the device for future space systems and missions. The ac Stark shift (i.e., light shift) is one of the more likely processes limiting the RAFS' long-term timekeeping ability, yet its manifestation in the RAFS remains poorly understood. In part, this comes from the fact that light-shift induced frequency fluctuations must be quantified in terms of the RAFS' light-shift coefficient *and* the output variations in the RAFS' rf-discharge lamp, which is a nonlinear inductively-couple plasma (ICP). Here, we analyze the light-shift effect for a family of 10 on-orbit Block-IIR GPS RAFS, examining decade-long records of their on-orbit frequency and rf-discharge lamp fluctuations. We find that the ICP's light intensity variations can take several forms: deterministic aging, jumps, ramps, and non-stationary noise, each of which affects the RAFS' frequency via the light shift. Correlating these light intensity changes with RAFS frequency changes, we estimate the light-shift coefficient, κ_{LS}, for the family of RAFS: $\kappa_{LS} = -(1.9 \pm 0.3) \times 10^{-12}/\%$. The 16% family-wide variation in κ_{LS} indicates that while each RAFS may have its own individual κ_{LS}, the variance of κ_{LS} among similarly designed RAFS can be relatively small. Combining κ_{LS} with our estimate of the ICP light intensity's non-stationary noise, we find evidence that random-walk frequency noise in high-quality space-borne RAFS is strongly influenced by the RAFS' rf-discharge lamp via the light shift effect. *Published by AIP Publishing.* [http://dx.doi.org/10.1063/1.4967787]

I. INTRODUCTION

Arguably, the rubidium atomic frequency standard (RAFS) is the workhorse of ultraprecise timekeeping in space.[1] Its low weight, small volume, low power consumption, high reliability,[2] and relative radiation insensitivity[3] make it attractive for a host of diverse space missions; and its frequency stability rivals that of larger and heavier passive hydrogen masers.[4,5] Consequently, Rb atomic clocks find application on Global Navigation Satellite System spacecraft (GNSS), for example, GPS,[6] BeiDou,[7] and Galileo;[8] they fly on communication system satellites,[2,9] and they are planned for deep space missions.[10]

Notwithstanding the RAFS' attractive characteristics and ubiquity, system and space mission planners are continually pushing for better performance from the device in order to meet stricter system and mission requirements. In particular, lower levels of stochastic frequency fluctuations (on time scales of 10^3 s and longer) and smaller rates of deterministic frequency aging are desired, since both determine the clock's ultimate timekeeping ability. Unfortunately, at the present time the mechanism(s) behind frequency aging in the RAFS remains unknown,[11] as does the stochastic process (or processes) driving the clock's random-walk frequency noise.[12,13] Consequently, without an understanding of the underlying mechanisms behind these processes, empirical engineering is the only path forward for Rb atomic clock improvement.

Of the many physical processes that could play a role in the Rb clock's long-term frequency stability,[14] the light shift (or ac Stark shift)[15,16] is high on the suspect list. (For example, with a temperature sensitivity of $\sim 4 \times 10^{-15}/^{\circ}\mathrm{C}$,[4] temperature variations of a GPS RAFS are likely of secondary importance.) Briefly, it is thought that low-level variations in the intensity and/or the spectrum of the lamplight entering the clock's resonance cell could produce relatively large time varying shifts in the ^{87}Rb atom's ground-state hyperfine splitting as a consequence of virtual (optical) photon absorption. Understanding the role that the light shift plays in the Rb clock's frequency stability therefore requires a more holistic approach to the problem then has been typical in the past. Not only is it necessary to have a better understanding of the magnitude and stability of the device's light-shift coefficient κ_{LS}, but also one must have a clear characterization of the magnitude and temporal behavior of the light's variations. Here, we examine the long-term frequency and light intensity histories of on-orbit GPS RAFS (histories that in many cases span more than a decade) in order to address three basic questions: (1) what is the constancy of the light-shift coefficient over time; (2) what is the manner of random

and deterministic light intensity variations for the Rb clock's rf-discharge lamp over the long term, and (3) what are the limitations that light intensity fluctuations place on the stability of high-quality space-borne Rb atomic clocks via the ac Stark shift?

In Section II, we give a brief overview of the Rb clock's functioning and the light shift in order to provide a context for what follows. Then, in Section III we examine the temporal signatures of light intensity variations for a family of GPS Block-IIR RAFS, cataloging these as: (a) deterministic light intensity aging, (b) light intensity jumps of random occurrence, (c) periodic light intensity ramps of unpredictable length and magnitude, and (d) continuous non-stationary light intensity noise. In Section IV, we correlate the light intensity variations with clock frequency variations in order to obtain on-orbit estimates of the various GPS RAFS' light-shift coefficients, and to consider the long-term constancy of the light-shift coefficient in these devices. Finally, in Section V, we examine the long-term frequency fluctuations of the GPS Rb clocks, and compare this to the frequency fluctuations inferred from lamplight intensity noise and the light-shift coefficient, arguing that lamplight intensity noise (via the ac Stark shift) plays a significant role in limiting the long-term frequency stability of high-quality space-borne Rb clocks.

II. THE RUBIDIUM ATOMIC CLOCK AND THE LIGHT SHIFT

A. Overview of the Rb Clock

Figure 1 shows the physics package of the generic Rb atomic clock: an rf-discharge lamp (i.e., an inductively coupled plasma or ICP), a filter cell, a resonance cell, and a photodetector, with the resonance cell inside a microwave cavity that is tuned to the ^{87}Rb atom's hyperfine resonance frequency at 6834.7 MHz. The Rb resonance light generated by the ICP passes through the filter cell, and in so doing has its optical spectrum "shaped"[17–19] so that it can efficiently produce an atomic signal via the optical-pumping process.[20] As a consequence of optical pumping, the steady-state population of atoms in the absorbing hyperfine level (i.e., $F=1$) is reduced, and so the Rb vapor in the resonance cell becomes (to some degree) transparent to the ICP light. With the Rb vapor absorbing little light, more passes through to the photodiode.

If microwaves are applied to the vapor at the hyperfine resonance frequency, atoms are forced by the microwave signal to return to the absorbing hyperfine state. Consequently, more light gets absorbed by the vapor, and less passes through to the photodiode. The change in transmitted light intensity corresponds to the amplitude of the atomic clock signal, which can be used in a feedback loop to lock the source of the microwave signal (e.g., a voltage-controlled crystal oscillator, VCXO, at ~10 MHz) to the atomic hyperfine resonance frequency.[14] The Rb resonance light from the ICP is, thus, crucial to the RAFS' operation, since it generates the atomic signal via optical pumping, and it monitors the atoms' absorption of the microwaves. The light also plays a role in defining the clock's output frequency via the ac Stark shift.

B. The ac stark shift or light shift

In semiclassical electrodynamics,[15,16] the light shift arises as a second-order interaction between an atom's induced dipole moment and the light's perturbing electric field. For present purposes, we consider the atom as a polarizable medium with a (frequency dependent) polarizability $\alpha(\omega)$. The perturbing electric field of the light, $\vec{E}(\omega)$, will then induce a dipole moment $\vec{p}(\omega)$ in the atom

$$\vec{p}(\omega) = \alpha(\omega)\vec{E}(\omega). \tag{1}$$

This dipole moment interacts in second-order with the electric field that produced it, thereby perturbing the atom's energy by $\delta\varepsilon$

$$\delta\varepsilon = -\frac{1}{2}\vec{p}(\omega)\cdot\vec{E}(\omega). \tag{2}$$

The perturbation of the atom's energy level structure manifests itself as a shift in the atom's ground-state hyperfine splitting, $h\nu_{hfs} = (\varepsilon_{F=2} - \varepsilon_{F=1})$

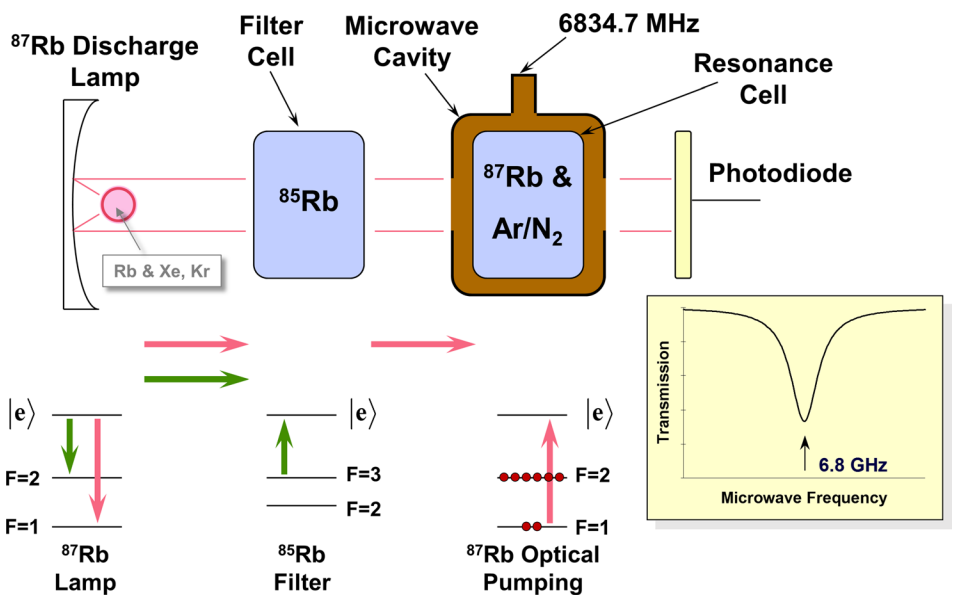

FIG. 1. Block diagram of the prototypical Rb atomic clock. The ^{87}Rb rf-discharge lamp (i.e., an inductively-coupled plasma) emits spectral lines that originate in a rubidium excited state and terminate on one of the two ground-state hyperfine levels of the atom (i.e., $F=2$ and $F=1$). Due to a coincidence of nature, one of these spectral lines is absorbed by the ^{85}Rb atoms in the resonance cell, allowing the other spectral line to pass through, where it can create a population imbalance between the ground-state hyperfine levels via optical pumping.

$$y_{LS} = \frac{\delta f}{f_o} = \frac{(\delta\varepsilon_{F=2} - \delta\varepsilon_{F=1})}{h\nu_{hfs}} = -\frac{\Delta\vec{p}(\omega)\cdot\vec{E}(\omega)}{2h\nu_{hfs}}$$
$$= -\left(\frac{|E(\omega)|^2}{2h\nu_{hfs}}\right)\Delta\alpha(\omega), \quad (3)$$

where $\Delta\alpha(\omega) = [\alpha_{F=2}(\omega) - \alpha_{F=1}(\omega)]$.

While the light shift expressed by Eq. (3) is valid for a monochromatic electromagnetic wave, it is important to recognize that the light emitted by the ICP is relatively broad band,[21–23] with each spectral component contributing to the overall fractional-frequency light shift via Eq. (3). Further, as illustrated in Fig. 1 the spectrum of the light from the ICP will be modified on passage through the filter cell,[17–19] and will also be affected by passage through the vapor of the resonance cell.[24] Thus, if we consider the atomic signal of the clock as generated within some local region of the resonance cell,[25,26] we can express the actual light shift of the clock in terms of a light-intensity attenuation factor after passage through the filter cell η, an attenuation factor for light propagation from the front of the resonance cell to the atomic-signal generating region ξ, and a normalized ICP Rb light spectrum *in the resonance cell* $S(\omega)$

$$y_{LS} = -\left(\frac{E_o^2\eta\xi}{2h\nu_{hfs}}\right)\int_0^\infty \Delta\alpha(\omega)\,S(\omega)\,d\omega, \quad (4a)$$

$$\int_0^\infty S(\omega)d\omega = 1. \quad (4b)$$

Taking $I = \eta\xi E_o^2$, we re-express Eq. (4a) as

$$y_{LS} = \beta I = -I\int_0^\infty \left(\frac{\Delta\alpha(\omega)}{2h\nu_{hfs}}\right)S(\omega)\,d\omega, \quad (5)$$

where β is the light-shift coefficient of the atomic clock. (Note that the actual sign of the light-shift coefficient depends on the integrated overlap of $\Delta\alpha(\omega)$ and $S(\omega)$; in general, the sign is immaterial to RAFS performance, since the quantity of real interest is the *magnitude* of any changes in y_{LS}.)

As a functional of $S(\omega)$, β will depend on the emission spectrum of the ICP, which gives β a dependence on the rf-power driving the discharge P_{rf}, and the rf-discharge lamp's temperature T_L. Through $S(\omega)$, β also depends on the spectral shaping properties of the filter cell (determined by the filter-cell temperature T_F), and quite likely, some spectral shaping properties of the resonance cell (determined by the resonance-cell temperature, T_R). Therefore, even for Rb clocks of the same design, we should expect variation in β, since the ICP, the filter cell, and the resonance cell will always have some family-wide variance in the parameters P_{rf}, T_L, T_F, and T_R. Further, we would not be too surprised to find that β is a slowly varying function of time, since we could reasonably anticipate long-term variations in P_{rf}, T_L, T_F, and/or T_R for a RAFS (certainly over the course of a RAFS' decade-long lifetime). The light intensity in the resonance cell I (equal to $\eta\xi E_o^2$), also depends on these parameters, since a change in P_{rf} or T_L can affect E_o^2, and variations in T_F and T_R affect η and ξ, respectively. It is, therefore, not unreasonable to suspect variations in the light shift arising from *both* β and I, especially when one is looking at RAFS behavior over decade-long time scales.

Equation (5) defines the clock's "full" light shift. However, we are typically not interested in the full light shift, but rather, variations in the light shift. More specifically, the "operational" light shift of a RAFS is defined as the change in clock frequency associated with a *change* in ICP light intensity, which we will label as δ_{LS}: when we observe a light-induced frequency change in a RAFS, we are not seeing the light shift transition from "off" to "on"; rather, we are seeing a change in the light shift from one value to another. Therefore, defining I_o as the average light intensity in the atomic-signal generating region of the clock's resonance cell, and $\Delta I(t)$ as a change in ICP light intensity, we have

$$\delta_{LS}(t) \equiv \beta(t)I_o\frac{\Delta I(t)}{I_o} = \kappa_{LS}(t)\frac{\Delta I(t)}{I_o}, \quad (6)$$

where κ_{LS} is the parameter routinely reported in the literature for a clock's light-shift coefficient, often in units of $\%^{-1}$. (Note that clock-to-clock comparisons among κ_{LS} values should be treated with caution, since κ_{LS} is proportional to I_o.[27]) If we further assume that β changes slowly in time, then it can be expanded in a Taylor series to first order yielding

$$\kappa_{LS}(t) = \beta_o I_o + I_o t\left.\frac{d\beta}{dt}\right|_0, \quad (7)$$

where β_o is the nominal light-shift coefficient of the RAFS. As will be discussed subsequently, on average the light-shift coefficient for the GPS Block-IIR Rb clocks has the value $\kappa_{LS} = -1.9\times10^{-12}/\%$.

Notwithstanding β's dependence on a number of ICP independent Rb clock operating parameters (e.g., T_F and T_R), it is our contention that the ICP's parameters are the most prone to variation. For example, the filter cell and resonance cell are passive devices in terms of their effect on I_o and $S(\omega)$, and their temperature stability is a matter of straightforward (though careful) engineering. Consequently, we expect little real variation in T_F and T_R, and any small variation that does occur will likely be continuous as opposed to abrupt (barring failures). However, the alkali rf-discharge lamp is a nonlinear device,[28] and its typical operating regime in a Rb atomic clock pushes it close to instability.[29]

III. CHANGES IN THE ICP LIGHT INTENSITY REACHING THE RAFS PHOTODETECTOR

A. ICP light intensity telemetry analysis

We obtained on-orbit light-telemetry data from 10 Block-IIR GPS RAFS. On average, the light intensity for a single RAFS was monitored over a period of 12 years, so that our data represent a unique resource for studying RAFS ICP light intensity variations and light shifts. Unfortunately,

in its raw form the light telemetry data is limited in resolution by the telemetry signal's bit-level quantization, Δ_q, and does not allow detection of the small light-shift-inducing variations that are of most interest. However, the telemetry signal also contains noise, which causes the telemetry signal to fluctuate randomly between quantized levels. The standard deviation of the telemetry noise normalized to Δ_q, which we will label as σ_x, was approximately ± 0.85. Consequently, to get below the quantization limit we averaged our light telemetry data over 24-h periods.

To illustrate the effect of random noise on the telemetry signal, and its potential for biasing our light-telemetry estimates, we can consider a telemetry signal, V_r, (prior to quantization) offset from its nearest quantized value by δv: $V_r = V_q + \delta v$. To proceed, we restrict δv to $\pm\Delta_q/4$, so that given our estimate of σ_x three quantized levels should provide a fair representation of the full range of possible observed telemetry values. Then, assuming normally distributed telemetry signal fluctuations prior to quantization, the average telemetry signal will be given by

$$\begin{aligned}\langle V_m\rangle = \; & V_{q-1}P\left(x+\frac{\delta v}{\Delta_q}\le -\frac{1}{2}\right)\\ & + V_q\left\{1-P\left(x+\frac{\delta v}{\Delta_q}\le -\frac{1}{2}\right)-P\left(x+\frac{\delta v}{\Delta_q}\ge \frac{1}{2}\right)\right\}\\ & + V_{q+1}P\left(x+\frac{\delta v}{\Delta_q}\ge \frac{1}{2}\right), \end{aligned} \tag{8a}$$

$$\langle V_m\rangle = V_q + \Delta_q\left\{P\left(x+\frac{\delta v}{\Delta_q}\ge \frac{1}{2}\right)-P\left(x+\frac{\delta v}{\Delta_q}\le -\frac{1}{2}\right)\right\}, \tag{8b}$$

where x is a mean-zero random variable with variance σ_x^2, and $P(z \ge a)$ is the probability for having $z \ge a$. Evaluating Eq. (8b) to find the bias, ε, in our estimate of V_r (normalized to Δ_q), we have

$$\begin{aligned}\varepsilon &= \left(\frac{\langle V_m\rangle - V_q}{\Delta_q}\right)-\frac{\delta v}{\Delta_q}\\ &= \frac{1}{2}\left\{\mathrm{Erf}\left[\frac{\frac{1}{2}+\frac{\delta v}{\Delta_q}}{\sigma_x\sqrt{2}}\right]-\mathrm{Erf}\left[\frac{\frac{1}{2}-\frac{\delta v}{\Delta_q}}{\sigma_x\sqrt{2}}\right]\right\}-\frac{\delta v}{\Delta_q}. \end{aligned} \tag{9}$$

The bias is shown in Fig. 2, and the magnitude of its mean value over the range of δv that we analyzed is $0.03\Delta_q$. Considering standard 8-bit quantization, this would imply an average ability to resolve normalized ICP light intensity variations at the 0.01% level (or better) without bias. (As other quantized levels are included in the analysis, the bias computed via generalizations of Eq. (8a) reduces in size.) Consequently, we will ignore any potential bias in our estimates of the light intensity telemetry in what follows.

B. Deterministic ICP light intensity variations

Figure 3 shows one example of the long-term deterministic trend of RAFS lamplight intensity; this data was obtained from GPS SVN-54. As is clear from the figure, the

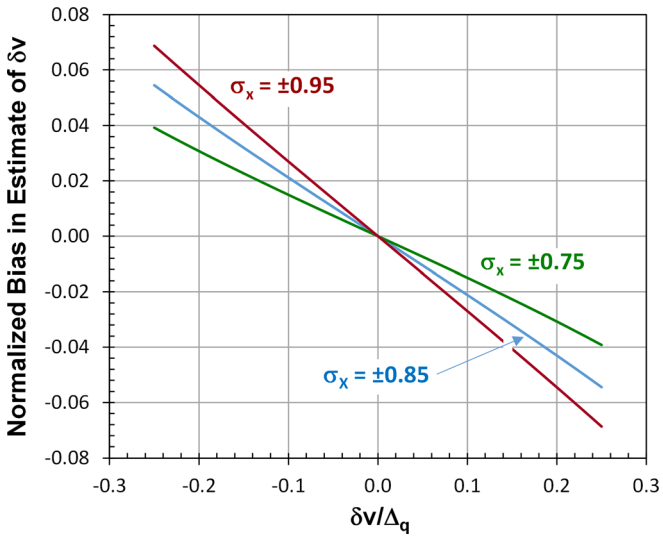

FIG. 2. Upper-bound estimate of the bias in our average of the lamplight telemetry signal resulting from averaging the quantized (i.e., digitized) signal. Our average relative noise on the quantized signal was $\sigma_x = \pm 0.85$, and varied between ± 0.75 and ± 0.95. These are upper-bound estimates of the bias, since our analysis only includes three quantized levels; the inclusion of other quantized levels lowers these bias values.

deterministic trend is reasonably well modeled by a decaying exponential sitting on a line

$$\frac{I(t)}{I_o} = Ae^{-\frac{t}{\tau}} + Bt + C. \tag{10}$$

All of the RAFS for which we have data show deterministic trends reasonably well-modeled by this form. The best fit coefficients for each of the RAFS are collected in Table I, and for the family of GPS Block-IIR RAFS we have

$$A = (1.21\pm 0.60)\%, \tag{11a}$$

$$B = -(0.078\pm 0.086)\%/\mathrm{yr}, \tag{11b}$$

$$C = (0.920\pm 0.075), \tag{11c}$$

$$\tau = (1.48\pm 0.46)\ \mathrm{yr}. \tag{11d}$$

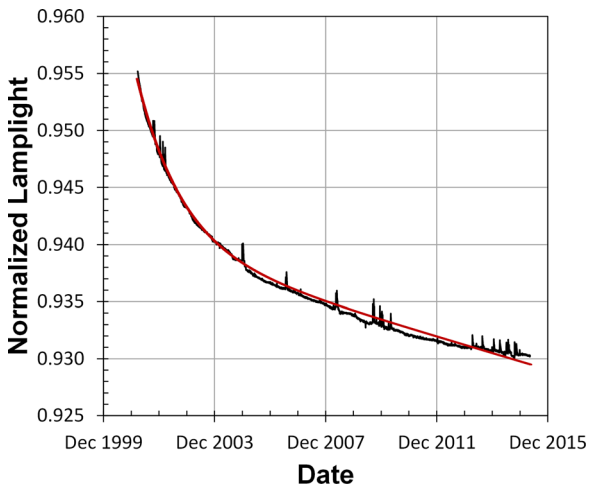

FIG. 3. Multiyear trend of normalized lamplight intensity (i.e., light level telemetry) from the RAFS onboard GPS SVN-54. The smooth line through the data is a fit to the form of Eq. (10).

TABLE I. Parameters for the deterministic model of RAFS long-term ICP light intensity variations.

SVN	A (%)	B (%/yr)	C	τ (yr)
41	1.13	+0.084	0.9893	2.2
43	0.42	−0.013	0.9931	1.8
44	1.00	−0.091	0.8328	0.9
46	2.54	−0.166	0.9336	1.3
49	0.59	−0.228	1.0011	0.9
50	1.19	−0.107	0.8211	1.5
51	0.93	−0.052	0.9927	1.4
54	1.48	−0.072	0.9398	1.6
60	1.10	−0.028	0.8677	2.1
61	1.69	−0.108	0.8304	1.1

As a consequence of the light-shift effect, one might reasonably assume that frequency aging in the RAFS is related to these deterministic ICP light-intensity trends. Briefly, combining Eqs. (6) and (10) (assuming $\dot{\beta} = 0$) and taking the derivative, one obtains

$$\dot{y}_{LS} = \kappa_{LS}\left(B - \left(\frac{A}{\tau}\right)e^{-\frac{t}{\tau}}\right). \tag{12}$$

Therefore, in the short term (i.e., $t \ll \tau$) one would predict for an ICP light-induced frequency aging rate

$$\dot{y}_{LS} = \kappa_{LS}\left(B - \frac{A}{\tau}\right) = +5.4 \times 10^{-15}\,\text{day}^{-1}, \tag{13a}$$

while in the long term one would predict

$$\dot{y}_{LS} = \kappa_{LS}B = +4.7 \times 10^{-16}\,\text{day}^{-1}. \tag{13b}$$

These, however, have the wrong sign and are at least an order of magnitude too small to account for the RAFS frequency aging that is actually observed on-orbit.[30] Thus, RAFS frequency aging would appear to be unrelated to deterministic ICP light (intensity) variations. That said, however, Eq. (13b) represents a lower bound to RAFS frequency aging: deterministic variations in the light intensity emitted by a RAFS' rf-discharge lamp limit its frequency aging to levels no lower than about 5×10^{-16}/day.

C. ICP light intensity jumps, ramps, and non-stationary noise

Superimposed on the deterministic trend of the light intensity emitted by the RAFS' ICP, there appear to be at least three distinct types of random variation: (1) light intensity jumps of random occurrence, (2) periodic light intensity ramps of unpredictable length and magnitude, and (3) continuous non-stationary ICP light intensity noise, which appears to be best characterized as either flicker noise or random-walk noise. Figures 4 and 5 show examples of ICP light intensity jumps and periodic ramps, respectively. Notice that the magnitudes of the ICP light intensity jumps are not insignificant: at levels ~0.15% they correspond to light-induced RAFS frequency jumps $\sim 3 \times 10^{-13}$ (using $|\kappa_{LS}| = 2 \times 10^{-12}$/%). Similarly, the amplitude of the periodic ICP light intensity ramps is ~0.05%, giving rise to light-induced RAFS frequency ramps of $\sim 1 \times 10^{-13}$.

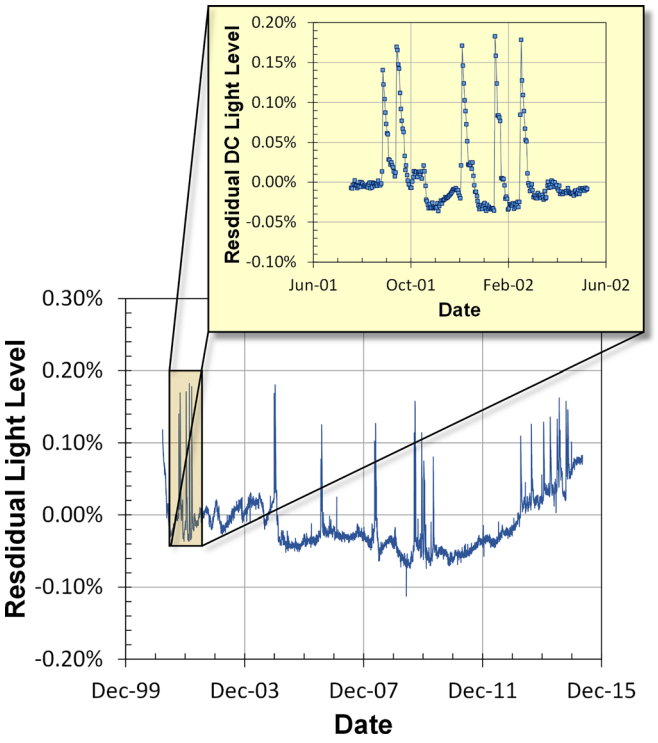

FIG. 4. Lamplight intensity jumps observed for the RAFS onboard SVN-54.

A number of the RAFS did *not* display clear ICP light intensity jumps nor clear periodic ICP light intensity ramps. They did, however, appear to show what can only be described as continuous non-stationary noise. Specifically,

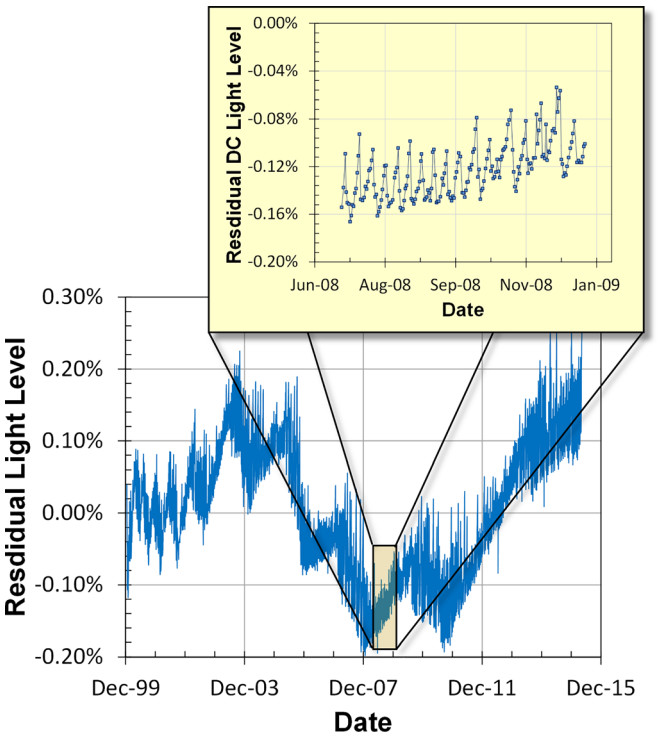

FIG. 5. Periodic lamplight intensity ramps observed for the RAFS onboard SVN-46.

we write the light intensity telemetry signal noise (after 24-h averaging) for the RAFS in the K^{th} space vehicle as

$$\zeta_K(t) = \left\{ \frac{I(t)}{I_o} - \left(A_K e^{-\frac{t}{\tau_K}} + B_K t + C_K \right) \right\} + x(t), \quad (14)$$

where x(t) is normally distributed measurement noise (independent of the ICP), which may (or may not) be stationary. Time series of ζ_K are shown in Fig. 6 for SVNs 43, 49, 60, and 61.

In order to estimate the Allan deviation of x(t), which we define as the "noise floor" of our light intensity measurements, we choose two quiescent periods in the data of Fig. 6: for SVN-49 the quiescent period was between days 1300 and 1550, and for SVN-61 between days 1650 and 1900. Though our actual ability to see random light intensity variations could be lower than our estimated noise floor, the estimated noise floor is certainly an upper bound on our true noise floor. The Allan deviation of $\zeta_K(t)$, $\sigma_\zeta(\tau)$, was then computed for the much longer data history. Specifically, due to gaps in the data we restricted our analysis of SVN-49 to $t > 400$ days, and SVN-43 to $t > 1000$ days. For SVN-60 and SVN-61 the full data record was employed in the Allan deviation computation. The results of the Allan deviation computation are shown in Fig. 7. As a consequence of the limitations imposed by our noise floor, we cannot say if the light intensity itself displays white noise for $\tau \leq 1$ day. However, it does appear that the ICP light intensity shows random-walk and perhaps flicker noise for $\tau > 10$ days. The two dashed lines passing through the data represent estimates of the ICP light intensity's Allan deviation, fit to the form $\sigma_\zeta(\tau) = \sqrt{a^2/\tau + b + c\tau}$. For the upper curve, we find $a = 4.0 \times 10^{-5}$, $b = 0$, and $c = 1.5 \times 10^{-5}$; for the lower curve we find $a = 4.5 \times 10^{-5}$, $b = 4.0 \times 10^{-5}$, and $c = 3 \times 10^{-6}$ (with τ in days).

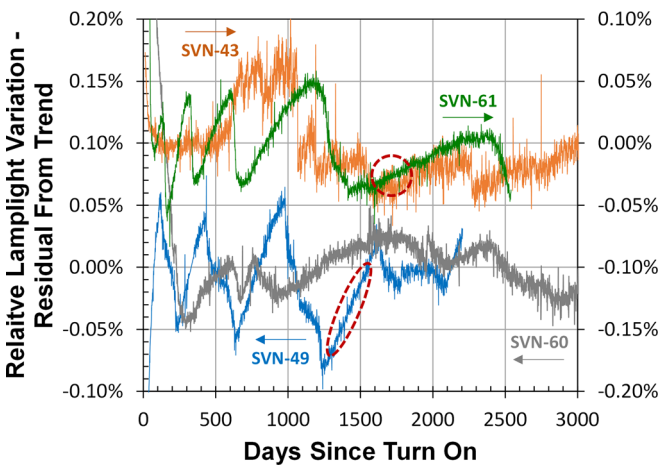

FIG. 6. Residual lamplight intensity variations for a number of GPS Block-IIR satellites that did not show clear lamplight intensity jumps or periodic lamplight intensity ramps. An upper bound to the measurement noise floor was computed using a portion of the $\zeta_K(t)$ time series for the RAFS onboard SVN-49 and SVN-61. These portions are circled by the dashed lines. Of course it might be argued that the lamplight intensity for SVN-49 and SVN-61 is showing something strikingly similar to periodic lamplight intensity ramps. For the present, since the period of these ramps is on the order of a year, we treat them as noise. However, prudence dictates that we keep ourselves open to a possible connection between these extremely slow (potential) ramps and the lamplight intensity ramps shown in Fig. 5.

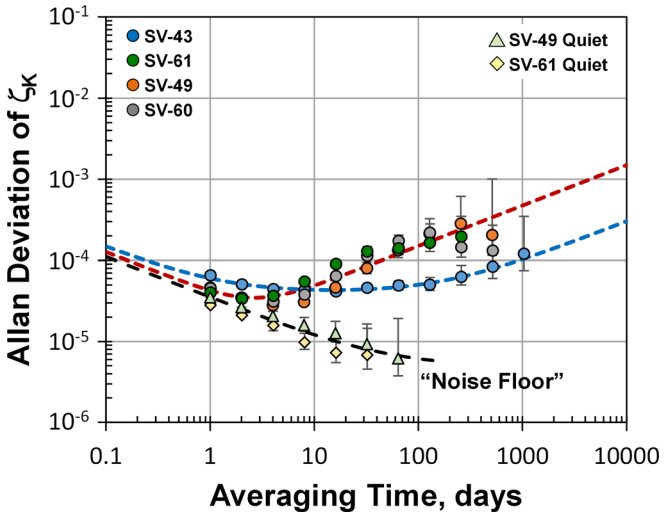

FIG. 7. Allan deviation of the residual lamplight intensity variations after subtracting the lamplight intensity's deterministic trend. The two dashed lines are fits, estimating the measurement noise floor and the lamplight intensity Allan deviation.

Before closing this section, we note that the ICP light intensity "jumps" illustrated in Fig. 4 might not be true discontinuous changes in light intensity. Since our data correspond to 1-day averages, all we can say regarding the jumps of Fig. 4 is that within a 24-h period the light intensity changed significantly. When or how long it took for the change to occur during that 24-h window we cannot say. Further, as illustrated in Fig. 1 our telemetry data actually corresponds to the ICP light intensity reaching the photodetector after passage through the filter cell and the resonance cell; and while we believe that all light intensity variations arise within the rf-discharge lamp, as opposed to the filter cell or resonance cell, our telemetry data alone do not unequivocally support that conjecture. Thus, the on-orbit data alone admits the possibility that the "jumps" might arise from continuous changes in T_F and/or T_R over the 24-h averaging window.

Fortunately, in a completely separate study where two of us (MH and JC) are collaborating on an experiment to evaluate GE-180 glass for RAFS rf-discharge lamps,[31] we have been able to observe light intensity jumps originating directly in an alkali ICP. Briefly, an important lamp failure mechanism in a RAFS is Rb consumption by the lamp bulb's glass walls.[32] With Corning 1720 glass no longer available for the lamps used in Rb clocks, the study is looking to quantify the consumption rate of Rb by GE-180 glass, which is a potential Corning 1720 replacement. As part of that study, the emission spectra for all of the lamps are recorded every 15 min (over the wavelength range 350 to 1020 nm). Our data records are routinely 30 days long with gaps of about a week when we assess the Rb consumption over the 30-day lamp operating time. While in operation, the rf-discharge lamps are open to the laboratory environment, and not actually housed in a RAFS.

Figure 8 shows two cases of rf-discharge lamp jumps observed in this separate study. The figures show the intensity of the 795 nm Rb light intensity and the 823 nm Xe light

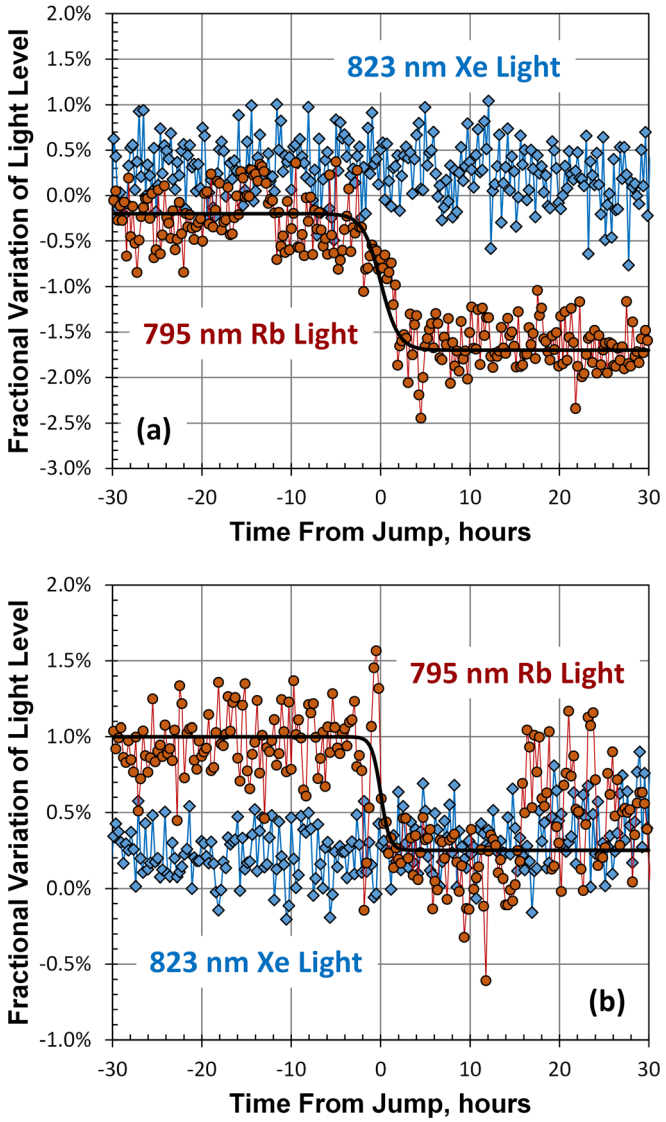

FIG. 8. Two examples of lamplight intensity jumps observed in the laboratory from a study aimed at measuring the Rb consumption rate for GE-180 glass. The solid line through the 795 nm Rb light intensity is a logistic function (i.e., $S_{795}(t) = S_o + \delta S/(1 + e^{t/\tau})$), whose parameters δS and τ characterize the jump: for the jump in (a) we have $\delta S = 1.5\%$ and $\tau = 1$ h, while for the jump in (b) we have $\delta S = 0.75\%$ and $\tau = 0.5$ h.

intensity, and as shown in the figure, the Rb light intensity jumps while the Xe light intensity remains constant. Constancy of the Xe light intensity implies that the change in Rb light intensity cannot be due to a systematic instability in the light-measurement system, as this would affect both the Rb light intensity and the Xe light intensity. Fitting the Rb light intensity change to a logistic function, the time scale of the jumps appears to be on the order of one hour or less, and the magnitudes of the jumps are ~1%. While these jump magnitudes are larger than those observed on orbit, their larger magnitudes might be a consequence of operating the ICPs in a laboratory environment as opposed to the carefully controlled environment inside a GPS RAFS. Regardless of these (in our opinion) slight discrepancies, the data of Fig. 8 provide independent evidence for light intensity jumps occurring in a RAFS' rf-discharge lamp, and suggest that the time scale of the jumps is much less than 24 h. In future work we will be analyzing these laboratory ICP light intensity histories more carefully, in the hopes of elucidating the mechanism driving rf-discharge lamp instability.

IV. ON-ORBIT LIGHT-SHIFT COEFFICIENTS

A. Estimation of κ_{LS} from on-orbit data

In order to estimate κ_{LS} from the on-orbit light telemetry and archived frequency-offset data, we employed two methods.[33] For the first, we correlated RAFS frequency jumps with observed ICP light intensity jumps. Specifically, given a light intensity jump at time t_i of a given duration, there will be a corresponding relative frequency jump, which then yields an estimate of the RAFS' light-shift coefficient $\hat{\kappa}_{LS}$

$$\hat{\kappa}_{LS} = \frac{\hat{\delta}_{LS}(t_i)}{\left(\frac{\Delta\hat{I}(t_i)}{I_o}\right)}. \tag{15}$$

Obviously, the larger the light intensity and frequency jumps relative to their respective noise levels, the better the estimate of $\hat{\kappa}_{LS}$. In what follows, we refer to this technique for estimating the light-shift coefficient as the "jump method."

The second method was more general, and made use of any type of deterministic ICP light intensity variation that resulted in a correlated frequency variation. The initial step in this method consisted of removing *un*correlated (or potentially uncorrelated) trends from the measured RAFS frequency and light intensity values. In particular, for those time periods when frequency aging and/or ICP light intensity aging changed with time (see for example, Fig. 3), we estimated and removed the aging for each time period over which it could be considered nearly constant. From Eq. (6) it follows that such detrended frequency and ICP light intensity data ($y_D(t)$ and $\Delta I(t)/I_o$, respectively) should satisfy

$$y_D(t) = \kappa_{LS}\frac{\Delta I(t)}{I_o} + \bar{y} + x(t) \tag{16}$$

if the detrended frequency is changing as a consequence of the light shift effect. Here, $\bar{y}$ is an average frequency offset of the RAFS over the particular time interval of correlation that is unrelated to the ICP light intensity (and not captured by the detrending), and x(t) is a noise term. Performing a least-squares linear fit between $y_D(t)$ and $\Delta I(t)/I_o$ over the time interval of apparent correlation, the slope becomes our estimate $\hat{\kappa}_{LS}$. Clearly, the closer the Pearson-product correlation coefficient r to ± 1, the better the estimate of $\hat{\kappa}_{LS}$. In what follows, we will refer to this technique for estimating the light-shift coefficient as the "correlation method."

As an illustration of the correlation method, Fig. 9(a) shows frequency and light intensity data for the operational RAFS on-board satellite SVN-46 for the period 1 January 2008 to 30 January 2014. Over the short term (10 days), the frequency and the light intensity show a similar periodic behavior, which can be used to estimate the light-shift coefficient via the correlation method. As noted, the first step is to estimate and remove the uncorrelated linear trends. Then, employing the detrended data we search for periods with

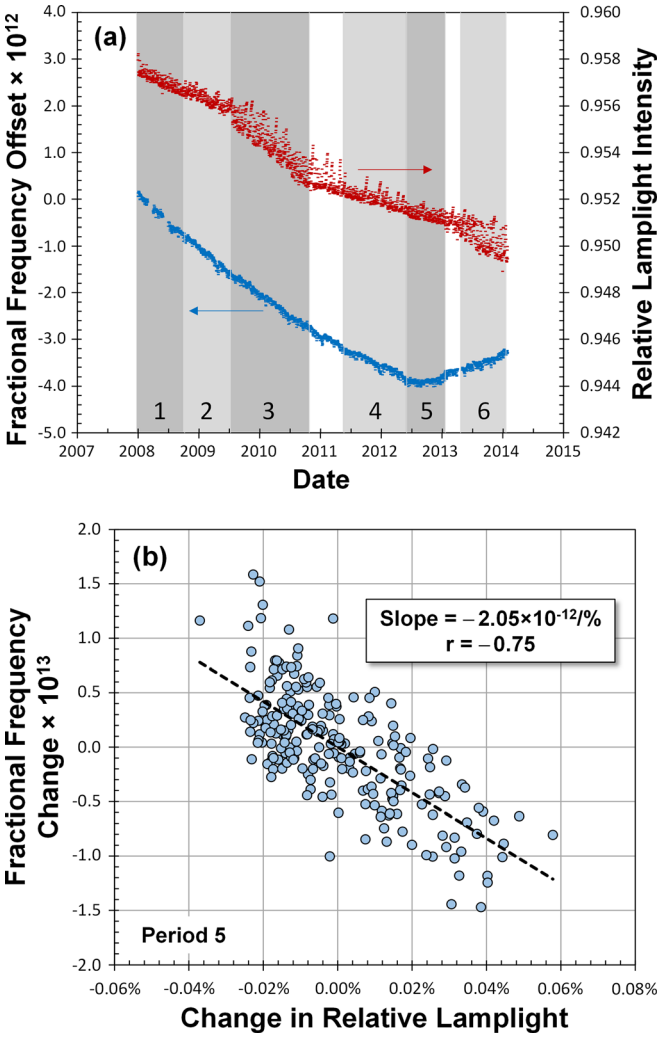

FIG. 9. (a) Fractional frequency deviation (lower) and normalized lamplight intensity (upper) histories for Block-IIR GPS SVN-46 between 1 January 2008 and 30 January 2014; various periods where significant frequency/lamplight correlation were found are indicated by the numbers one through six. (b) After detrending the data of (a), this figure shows the correlation between fractional frequency change (relative to the trend line) and lamplight intensity change for period 5.

"high" correlation between light intensity variations and frequency variations. Specifically, we looked for periods when the absolute value of the Pearson-product correlation coefficient was larger than 0.5. Though chosen somewhat arbitrarily, this threshold value is often taken as indicative of a reasonably large effect when data may be influenced by many factors.[34] For each of the selected periods, we then computed $\hat{\kappa}_{LS}$ via Eq. (16), with the standard error of the slope as our estimate of the uncertainty in $\hat{\kappa}_{LS}$. As a further check against accepting errant light-shift coefficient values, we only accepted those estimates of $\hat{\kappa}_{LS}$ whose value was non-zero at a 95% confidence level. For the data of Fig. 9(a), we found six periods satisfying our constraints, and the correlation for one of those periods is shown in Fig. 9(b).

B. Time variation of the light-shift coefficient

In previous work, Camparo hypothesized that changes in a RAFS' light-shift coefficient might be responsible for frequency aging.[30] Briefly, if we define the linear frequency aging rate D, of a RAFS through $y(t) = Dt$, then according to Camparo's hypothesis and Eq. (7) we should have

$$D = \dot{y}_{LS} = \dot{\beta} I_o = \dot{\kappa}_{LS} = \left(\frac{d\beta}{dt}\right)_{t=0} I_o. \tag{17}$$

To examine this hypothesis, we used the jump method to estimate the light-shift coefficient for GPS Block-IIR SVN-41, which is a RAFS for which we have our longest set of light-shift coefficient values. These are shown in Fig. 10, and span over a decade. In order to create such a long record of on-orbit light-shift coefficient determinations, we combined our estimates of light-induced frequency jumps (post 2007) with those recorded by Epstein *et al.* (2001 to 2005).[35]

As noted by Camparo,[30] $D_{SVN\text{-}41} = -3.75 \times 10^{-14}$/day, and from Eq. (17) this frequency aging rate would require $\dot{\kappa}_{LS} = -1.37 \times 10^{-13}/(\% \cdot \text{yr})$. However, this value is much larger than the slope of the regression line for the data of Fig. 10: $\dot{\kappa}_{LS} = +(0.27 \pm 0.56) \times 10^{-13}/(\% \cdot \text{yr})$. Specifically, employing the standard error of $\dot{\kappa}_{LS}$, the probability for this RAFS' frequency aging to be due to a temporal change of the light-shift coefficient is only 0.0017 (i.e., the probability that $\dot{\kappa}_{LS} \leq D_{SVN\text{-}41}$, noting that $D_{SVN\text{-}41}$ is negative). Thus, the data from this particular RAFS does not support Camparo's hypothesis. Moreover, considering the change in the light-shift coefficient for SVN-46, obtained from the data shown in Fig. 9(a), we get $\dot{\kappa}_{LS} = -(0.4 \pm 1.6) \times 10^{-13}/(\% \cdot \text{yr})$. While the uncertainty in $\dot{\kappa}_{LS}$ for SVN-46 is larger than that of SVN-41 (as a consequence of its shorter data length), the null result is consistent with SVN-41. Thus, it is our opinion that these data cast extreme doubt on the notion that $D = \dot{\kappa}_{LS}$.

C. RAFS-to-RAFS variation of κ_{LS}

In total, we were able to estimate light-shift coefficients for eight Block-IIR GPS RAFS. These are collected in Table II, and plotted in Fig. 11. All of the RAFS had negative light-shift coefficients, and as suggested by the data of Fig. 11 each RAFS appears to have its own unique light-shift

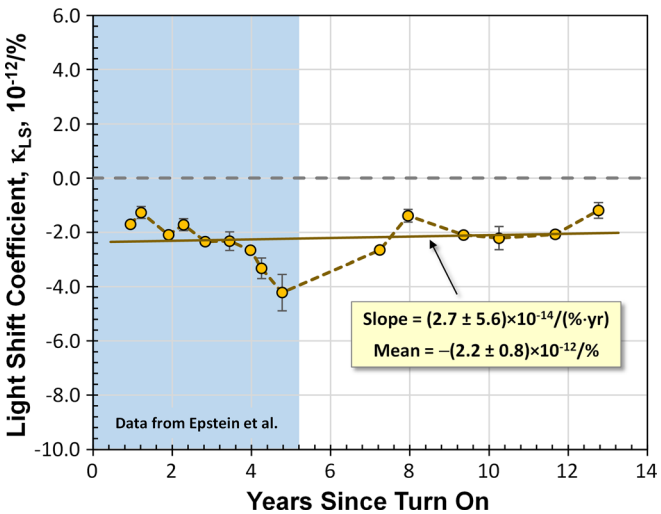

FIG. 10. History of light-shift coefficient values for GPS Block-IIR SVN-41.

TABLE II. Estimated light-shift coefficients for a number of Block-IIR GPS RAFS.

SVN	Estimation method	Number of estimated κ_{LS}	$\langle\kappa_{LS}\rangle$ ($\%^{-1}$)	Standard error ($\%^{-1}$)
41	Jump	15	-2.22×10^{-12}	0.21×10^{-12}
43	Correlation, $r_{rms}=-0.57$	5	-2.00×10^{-12}	0.30×10^{-12}
44	Correlation, $r_{rms}=-0.60$	5	-0.91×10^{-12}	0.15×10^{-12}
46	Correlation, $r_{rms}=-0.66$	6	-1.52×10^{-12}	0.19×10^{-12}
49	Correlation, $r=-0.99$	1	-3.34×10^{-12}	0.16×10^{-12}
50	Correlation, $r=-0.66$	1	-1.73×10^{-12}	0.09×10^{-12}
54	Jump	10	-0.85×10^{-12}	0.18×10^{-12}
61	Correlation, $r=-0.56$	1	-2.43×10^{-12}	0.65×10^{-12}

coefficient (error bars are estimates of the 95% confidence intervals). This of course makes sense, as E_o^2, η, ξ, and $S(\omega)$ can all be expected to have variance about some family-wide average value. Further, though we were only able to estimate the light-shift coefficient using the jump method for two RAFS, there appears to be no systematic variation in $\hat{\kappa}_{LS}$ for the jump and correlation methods. Taken together, the family-wide average value of κ_{LS} is $-1.9\times10^{-12}/\%$ with a family-wide standard deviation of $\pm0.3\times10^{-12}/\%$.

V. SUMMARY AND DISCUSSION

As noted previously, in order to understand the role of the light shift in high-quality space-borne RAFS, it is necessary to know the RAFS' light-shift coefficient *and* the forms of possible ICP light intensity variations. Barring the deterministic ICP light-level trend, for which we have fairly consistent data across the family of Block-IIR GPS RAFS, we presently have only a catalogue of various types of stochastic ICP light intensity behavior: light intensity jumps, light intensity ramps, and non-stationary light intensity noise. In future work, we intend to examine the statistical properties of this data in more detail, and hopefully gain a fuller description. Nevertheless, there are several statements we can make at the present time regarding the light shift in high-quality space-borne RAFS:

(1) The deterministic light-level trend of a RAFS' rf-discharge lamp plays no role in the frequency aging of present-day RAFS. That said, however, the deterministic light-level trend does place a lower bound on frequency aging: $\sim5\times10^{-16}$/day.
(2) Jumps and ramps in the light level coming from the RAFS' inductively-coupled plasma (i.e., the rf-discharge lamp used for optical pumping) make their appearance in the RAFS' output frequency at levels on the order of 10^{-13}. These could be reduced in size by making the inductively-coupled plasma quieter and/or the RAFS' light-shift coefficient smaller.
(3) Non-stationary rf-discharge lamp noise *must* play a role in setting a lower limit to the RAFS' long-term frequency stability via the light shift.

With regard to this last point, we can actually go a bit further. Based on the data shown in Fig. 7 for SVN-49, SVN-60, and SVN-61, we expect the ICP light intensity from a high-quality RAFS to show random-walk behavior: $\sigma_\xi(\tau)=5.1\times10^{-8}\,\tau^{1/2}$, where τ is now in seconds. Combining this Allan deviation of the light intensity with the family-wide RAFS light-shift coefficient, we obtain an estimate of the ICP light-*inferred* Allan deviation of the RAFS, $\kappa_{LS}\sigma_\xi(\tau)$. This is shown in Fig. 12, along with the results of the actual performance of

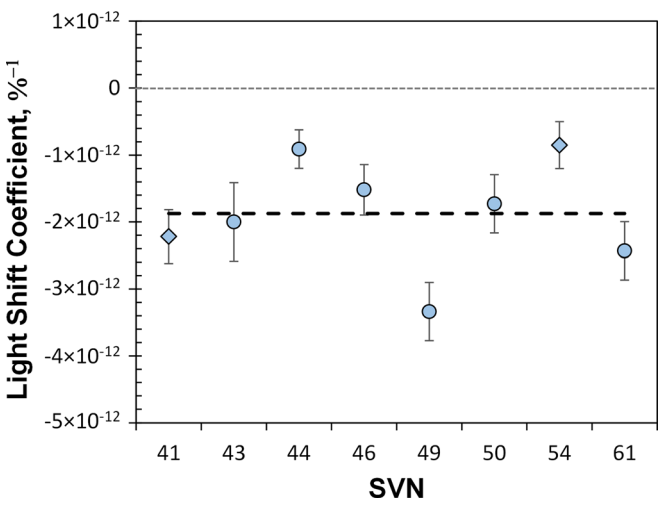

FIG. 11. Estimates of κ_{LS} for eight Block-IIR GPS RAFS. Diamonds correspond to κ_{LS} estimated via the jump method, while circles correspond to κ_{LS} estimated via the correlation method. The long dashed line in the figure is the family-wide average, and error bars correspond to estimates of the 95% confidence interval.

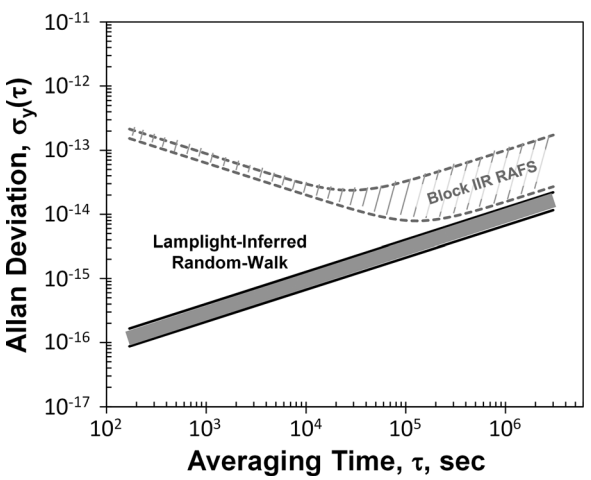

FIG. 12. Dashed lines correspond to manufacturer estimates of the performance of the GPS Block-IIR RAFS. The dark grey region is our estimate of the lamplight-inferred random-walk frequency noise.

the Block-IIR GSP RAFS measured on the ground by the manufacturer.[4] In the figure, the dark grey region corresponds to a 95% confidence interval for the family-wide variability of κ_{LS}. The data clearly suggest that the long-term stability of these high-quality RAFS is significantly influenced by the random variability of the light intensity from the rf-discharge lamp. If further analyses reach the same conclusion, it would point the way to a major improvement in high-quality space-borne RAFS. It would suggest that the random-walk frequency noise of a RAFS can be significantly lessened by making the rf-discharge lamp quieter and/or reducing the RAFS' light-shift coefficient. For such an improved RAFS, the data of Fig. 12 suggest the possibility of a RAFS breaking into the 10^{-16} frequency stability range, which would certainly result in new and novel concepts for space systems, and enhanced capabilities for deep-space missions.

ACKNOWLEDGMENTS

J. Camparo's efforts were funded by U.S. Air Force Space and Missile Systems Center under Contract No. FA8802-14-C-0001.

[1]J. Camparo, "The rubidium atomic clock and basic research," Phys. Today **60**(11), 33–39 (2007).
[2]J. Camparo, J. O. Hagerman, and T. A. McClelland, "Long-term behavior of rubidium clocks in space," in *Proceedings of the European Frequency and Time Forum* (IEEE Press, Piscataway, NJ, 2012), pp. 23–27.
[3]J. C. Camparo, S. C. Moss, and S. D. LaLumondiere, "Space-system timekeeping in the presence of solar flares," IEEE Aerosp. Electron. Syst. Mag. **19**(5), 3–8 (2004).
[4]R. T. Dupuis, T. J. Lynch, and J. R. Vaccaro, "Rubidium frequency standard for the GPS IIF program and modifications for the RAFSMOD program," in *Proceedings of the IEEE International Frequency Control Symposium* (IEEE Press, Piscataway, NJ, 2008), pp. 655–660.
[5]F. Droz, P. Mosset, G. Barmaverain, P. Rochat, Q. Wang, M. Belloni, L. Mattioni, U. Schmidt, T. Pike, F. Emma, P. Waller, and G. Gatti, "Galileo rubidium standard and passive hydrogen maser – Current status and new development," in *Satellite Communications and Navigation Systems*, edited by E. Del Re and M. Ruggieri (Springer Science + Business Media, New York, NY, 2008), pp. 133–139.
[6]W. Marquis, "Increased navigation performance from GPS Block IIR," Navigation **50**(4), 219–233 (2003).
[7]C. Han, Y. Yang, and Z. Cai, "BeiDou navigation satellite system and its time scales," Metrologia **48**, S213–S218 (2011).
[8]P. Waller, F. Gonzalez, S. Binda, I. Sesia, I. Hidalgo, G. Tobias, and P. Tavella, "The in-orbit performances of GIOVE clocks," IEEE Trans. Utrason. Ferroelectr. Freq. Control **57**(3), 738–745 (2010).
[9]J. C. Camparo, R. P. Frueholz, and A. P. Dubin, "Precise time synchronization of two Milstar communications satellites without ground intervention," Int. J. Sat. Commun. **15**, 135–139 (1997).
[10]S. Klioner, "High-accuracy timing for Gaia data from one-way time synchronization," Proc. J. 2014 **1**, 55–60 (2015).
[11]J. C. Camparo, "A partial analysis of drift in the rubidium gas cell atomic frequency standard," in *Proceedings of the 18th Annual Precise Time and Time Interval (PTTI) Applications and Planning Meeting* (United States Naval Observatory, Washington D. C., 1986), pp. 565–586.
[12]C. H. Volk and R. P. Frueholz, "The role of long-term lamp fluctuations in the random walk of frequency behavior of the rubidium frequency standard: A case study," J. Appl. Phys. **57**(3), 980–983 (1985).
[13]R. P. Frueholz, "The effects of ambient temperature fluctuations on the long term frequency stability of a miniature rubidium atomic frequency standard," in *Proceedings of the IEEE International Frequency Control Symposium* (IEEE Press, Piscataway, NJ, 1996), pp. 1017–1022.
[14]J. Vanier and C. Audoin, *The Quantum Physics of Atomic Frequency Standards* (Adam Hilger, Bristol, England, 1989), Vol. 2, Chap. 7.
[15]S. Pancharatnam, "Light shifts in semiclassical dispersion theory," J. Opt. Soc. Am. **56**(11), 1636 (1966).
[16]B. S. Mathur, H. Tang, and W. Happer, "Light shifts in the alkali atoms," Phys. Rev. **171**(1), 11–19 (1968).
[17]T. Tako, Y. Koga, and I. Hirano, "Absorption of Rb-D lines by Rb filter cell," Jpn. J. Appl. Phys., Part 1 **14**(11), 1641–1646 (1975).
[18]N. Kuramochi, I. Matsuda, and H. Fukuyo, "Analysis of the effect of foreign gases in the filtering action of a ^{85}Rb cell," J. Opt. Soc. Am. **68**(8), 1087–1092 (1978).
[19]J. Vanier, R. Kunski, P. Paulin, M. Tetu, and N. Cyr, "On the light shift in optical pumping of rubidium 87: The techniques of "separated" and "integrated" hyperfine filtering," Can. J. Phys. **60**, 1396–1403 (1982).
[20]W. Happer, "Optical pumping," Rev. Mod. Phys. **44**(2), 169–249 (1972).
[21]V. B. Gerard, "Laboratory alkali metal vapour lamps for optical pumping experiments," J. Sci. Instrum. **39**, 217–218 (1962).
[22]R. J. Atkinson, G. D. Chapman, and L. Krause, "Light sources for the excitation of atomic resonance fluorescence in potassium and rubidium," J. Opt. Soc. Am. **55**(10), 1269–1274 (1965).
[23]N. Kuramochi, I. Matsuda, N. Oura, and H. Fukuyo, "Analysis of the temperature dependence of 87Rb lamp profiles," J. Opt. Soc. Am. **70**(12), 1504–1507 (1980).
[24]G. Busca, M. Têtu, and J. Vanier, "Light shift and light broadening in the ^{87}Rb maser," Can. J. Phys. **51**(13), 1379–1387 (1973).
[25]A. Risley, S. Jarvis, and J. Vanier, "The dependence of frequency upon microwave power of wall-coated and buffer-gas-filled gas cell Rb^{87} frequency standards," J. Appl. Phys. **51**(9), 4571–4576 (1980).
[26]J. C. Camparo and R. P. Frueholz, "A three-dimensional model of the gas cell atomic frequency standard," IEEE Trans. Ultrason. Ferroelectr. Freq. Control **36**(2), 185–190 (1989).
[27]J. C. Camparo, "Light-shifts of an integrated filter-cell rubidium atomic clock," Aerospace Report No. TOR-2015-02236 (The Aerospace Corporation, El Segundo, CA, 2015).
[28]J. Camparo, F. Wang, W. Lybarger, and Y. Chan, "A complex permeability model of rf-discharge lamps," in *Proceedings of the Precise Time and Time Interval (PTTI) Systems and Applications Meeting* (Institute of Navigation, Manassas, VA, 2013), pp. 62–68.
[29]J. Coffer, N. Encalada, M. Huang, and J. Camparo, "Low-frequency, self-sustained oscillations in inductively coupled plasmas used for optical pumping," J. Appl. Phys. **116**, 163301 (2014).
[30]J. Camparo, "Does the light shift drive frequency aging in the rubidium atomic clock?," IEEE Trans. Ultrason., Ferroelectr., Freq. Control **52**, 1075–1078 (2005).
[31]C. M. Klimcak, M. Huang, and J. C. Camparo, "Alkali metal consumption by discharge lamps fabricated from GE-180 aluminosilicate glass," in *Proceedings of the Joint Conference of the IEEE International Frequency Control Symposium and the European Frequency and Time Forum* (IEEE, Piscataway, NJ, 2015), pp. 180–187.
[32]C. H. Volk, R. P. Frueholz, T. C. English, T. J. Lynch, and W. J. Riley, "Lifetime and reliability of rubidium discharge lamps for use in atomic frequency standards," in *Proceedings of the 38th Annual Frequency Control Symposium* (IEEE Press, Piscataway, NJ, 1984), pp. 387–400; R. A. Cook and R. P. Frueholz, "An improved rubidium consumption model for discharge lamps used in rubidium frequency standards," in *Proceedings of the 42nd Annual Frequency Control Symposium* (IEEE Press, Piscataway, NJ, 1988), pp. 525–531.
[33]V. Formichella, J. Camparo, and P. Tavella, "Light-shift coefficient in GPS rubidium clocks: Estimation methods using lamplight/frequency correlations," in Proceedings of the European Frequency and Time Forum (2016).
[34]J. Cohen, "A power primer," Psych. Bull. **112**(1), 155–159 (1992).
[35]M. Epstein, T. Dass, J. Rajan, and P. Gilmour, "Long-term clock behavior of GPS IIR satellites," in *Proceedings of the 39th PTTI* (US Naval Observatory, Washington DC, 2007), pp. 59–78.